Exciton effects in sequential resonant tunneling of photocarriers in GaAs/AlAs multiple quantum wells

Harald Schneider and Joachim Wagner
Fraunhofer-Institut für Angewandte Festkörperphysik, Tullastrasse 72, D-79108 Freiburg, Germany

Klaus Ploog
Paul-Drude-Institute für Festkörperelektronik, Hausvogteiplatz 5-7, D-10117 Berlin, Germany
(Received 18 February 1993)

We have studied the sequential resonant tunneling characteristics of coupled GaAs/AlAs quantum wells (QW's) by measuring the electric-field dependence of the photocurrent and of the excitonic photoluminescence (PL) associated with the first and second conduction subband. If the first subband of a QW is resonantly aligned with the second subband of the adjacent QW, a maximum of the photocurrent, a strong reduction of the PL intensity from the first subband, and a pronounced enhancement of the PL associated with the second subband are observed. Unexpectedly, these resonant extrema are observed at different electric fields. This phenomenon is attributed to the different binding energies of the intrawell and interwell excitons.

I. INTRODUCTION

Recently, there has been considerable interest in tunneling phenomena between coupled multiple quantum wells (MQW's) in an electric field. In *strongly coupled* MQW structures (or superlattices), the interwell coupling between subbands results in a delocalization of the electronic wave functions. This delocalization gives rise to line splittings in the spectral dependence of the optical absorption and of the photocurrent. The most intriguing observation of this kind has been the demonstration of the Wannier-Stark localization of electronic minibands.[1,2] Resonant alignment between different subbands of adjacent wells also induces a line splitting.[3–5] In this case, the splitting is observed in transitions involving both the first and second subbands. It has been shown by Fox *et al.*[3,5] that the resonance field, where this line splitting is most pronounced, depends on the particular excitonic transition under study. The reason for this effect arises from differences between the binding energies of the participating excitons. This difference in binding energy alters the precise value of the resonance field.

In *weakly coupled* MQW's, the (homogeneous) width of the transitions involved exceeds the expected line splitting. Therefore, a line splitting due to resonantly aligned subband energies cannot be observed. Instead, coupling between adjacent wells results in a resonant enhancement of the transport rates, if the electric field is such that subband energies of adjacent wells are in resonance. This phenomenon has been investigated by field-dependent measurements of the photoluminescence (PL) intensity,[6–8] the transient photocurrent,[8–10] the PL decay time,[11] and optical pump-probe experiments.[12] In addition, as has been shown recently,[13,14] this transport effect induces an increase of the carrier population of the excited subband, thus giving rise to optical emission from excitons involving the excited subband. This emission is strongly enhanced at resonance. Such an emission experiment was used previously[13,14] to determine the intersubband relaxation time with subpicosecond accuracy.

In the present work, we report on a detailed study of the electric-field-dependent photoluminescence intensity due to excitonic recombination involving the first heavy hole and first conduction subbands ($e1$-$h1$) and the first heavy hole and second conduction subbands ($e2$-$h1$) of weakly coupled GaAs/AlAs MQW's. If the field is such that the lowest two subbands $e1$ and $e2$ of neighboring wells are energetically aligned, we observe a resonant decrease of the $e1$-$h1$ intensity and a resonant enhancement of the $e2$-$h1$ transition. The extrema of these resonance effects are observed at different fields. We show that, although the situation is different from the coherent regime, this difference can be traced back to excitonic effects. This phenomenon gives insight into the role of intrawell and interwell excitons on tunneling-related phenomena.

II. EXPERIMENTAL

This study was performed on an undoped MQW structure with 50 GaAs quantum wells of 12.3 nm width separated by 2.1-nm AlAs barriers. The MQW is sandwiched between 30-nm-thick layers of GaAs followed by 600-nm-wide $Al_{0.5}Ga_{0.5}As$ window layers. The $Al_{0.5}Ga_{0.5}As$ layers are n doped at the substrate side and p doped at the top side, respectively, both to about 5×10^{17} cm^{-3}. A p-doped GaAs cap was grown on top. The structure was grown by molecular-beam epitaxy on a (100)-oriented n^+ substrate and processed into mesas of 300 μm diameter with ring-shaped Ohmic contacts. 647.1-nm radiation from a c.w. Kr-ion laser was focused onto the sample with a spot size of about 200 μm. The PL was detected using a triple monochromator equipped with an intensified Si-diode array detector. The electric field F was calculated from the applied voltage V by using the equation $F=\alpha(V-V_{bi})/L$, with the MQW thickness

0163-1829/93/48(15)/11051(6)/$06.00

$L=0.78$ μm and the built-in voltage $V_{bi}=1.55$ V. The field-screening parameter α was determined from the intensity dependence of the resonance field. We obtained $\alpha=0.95$ and 0.76 at excitation powers of 0.06 and 0.3 mW, respectively. These values also gave satisfactory agreement between the field dependences of the $e1$-$h1$ wavelength at different excitation powers.

III. EXPERIMENTAL RESULTS

A. Photoluminescence intensity

Figure 1 shows a series of PL spectra in the spectral regions of the $e1$-$h1$ [Fig. 1(a)] and the $e2$-$h1$ [Fig. 1(b)] transitions at different electric fields and an excitation power of 0.3 mW. In Fig. 1(a), the $e1$-$h1$ transition appears at 1.539 eV at small fields and is Stark shifted with increasing field (1.508 eV at 116 kV/cm). Additional features, not to be further discussed here, arise from the thermally populated light-hole–exciton transition and from an impurity-related transition (about 11 meV above and 26 meV below the $e1$-$h1$ transition, respectively). In Fig. 1(b), the $e2$-$h1$ transition is observed at 1.617 eV (60 kV/cm). Resonant alignment between the lowest two conduction subbands $e1$ and $e2$, which occurs at around 60 kV/cm, causes a strong reduction of the $e1$-$h1$ PL intensity and a pronounced enhancement of the $e2$-$h1$ signal. A discussion of this resonance phenomenon including exciton effects is given below (see also Fig. 5).

The detailed field dependence of the $e1$-$h1$ and $e2$-$h1$ PL intensities, as obtained by a numerical integration of the PL spectra, is shown in Figs. 2(a) and 2(b) for two different excitation intensities. In both cases, the resonance maximum of the $e2$-$h1$ luminescence is observed to occur at clearly smaller fields than the resonance minimum of the $e1$-$h1$ luminescence. As indicated by the dashed lines, the difference between these resonance fields in Fig. 2 is about 7 kV/cm at 0.06 mW and 5 kV/cm at 0.3 mW excitation power. For further purpose we will use the average value of 6 kV/cm. Essentially the same resonance fields as observed for the PL intensities are also obtained for the occupation densities of the $e1$ and $e2$ subbands, since the field dependence of the oscillator strengths[13,14] (see below) of these transitions is comparatively weak.

In addition to the pronounced structure arising from the $e1$-$e2$ resonance, the data of Fig. 2(b) contain some

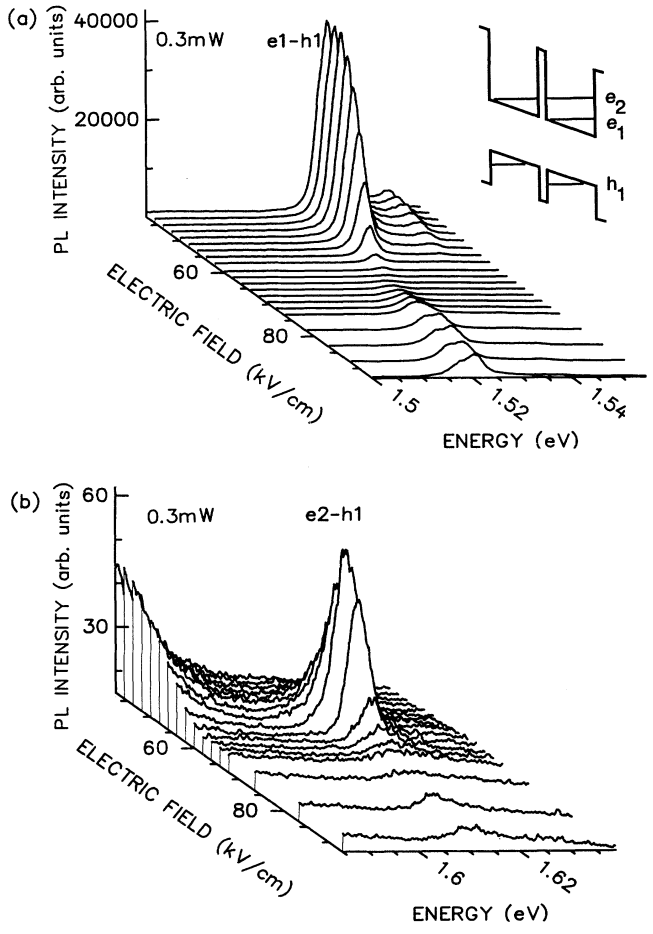

FIG. 1. Quasi-3D plot of PL spectra showing the spectral regions of the (a) $e1$-$h1$ and (b) $e2$-$h1$ transitions as a function of electric field. The spectra were excited with an optical power of 0.3 mW, corresponding to about 1W/cm^2. The subbands are indicated in the inset.

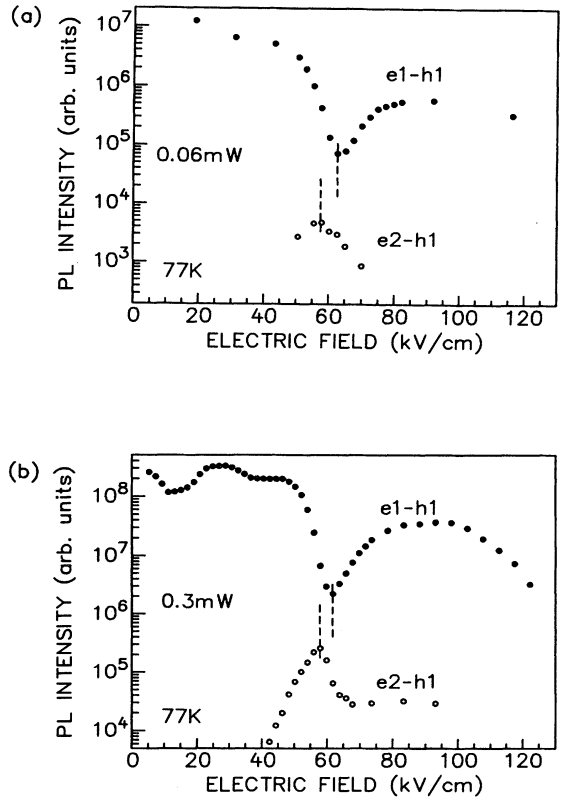

FIG. 2. PL intensities of the $e1$-$h1$ and $e2$-$h1$ transitions at (a) 0.06 mW and (b) 0.3 mW excitation power versus electric field. The dashed lines indicate the resonance extrema.

weaker structures at small fields. The minimum of the $e1$-$h1$ intensity appearing at 10 kV/cm arises from miniband conduction. The dip at 35 kV/cm, which corresponds to a potential drop of about 50 meV per MQW period, is probably associated with inelastic tunneling between the $e1$ subbands of adjacent wells, assisted by AlAs-like longitudinal-optical phonons. We note that these field values are influenced by space charges since our assumption of a constant field screening parameter underestimates space-charge effects at these small fields where the PL intensity is close to saturation. At high fields, the $e1$-$h1$ intensity drops again because of the nearby $e1$-$e3$ resonance occurring at around 150 kV/cm.[9,10,13] In addition, nonresonant tunneling processes become more and more important with increasing field.

B. Photocurrent

Additional information on the transport characteristics is obtained from the field dependence of the photocurrent, which is plotted in Fig. 3. Under constant illumination power, the photocurrent is a function of the ratio between the transport rate and the recombination rate. The photocurrent saturates when the transit time of the photoexcited carriers is much smaller than the recombination time. So the photocurrent as a function of the electric field shows only weak structure when the transit time is very short. However, a maximum in the field-dependent photocurrent still corresponds to a maximum in the ratio between the transport rate and the recombination rate. The inset of Fig. 3 illustrates the resonance situation of interest here, namely, the resonant alignment of the energies E_{e1}, E_{e2} of the $e1$ and $e2$ subbands. With the MQW period d, the resonance condition reads as

$$eFd = E_{e2} - E_{e1} \ . \tag{1}$$

From Fig. 3, we find an experimental field value of 60 kV/cm corresponding to this condition. This value lies in between the resonance fields as obtained from the $e1$-$h1$ PL and the $e2$-$h1$ PL. This result seems very reasonable since the field for maximum photocurrent

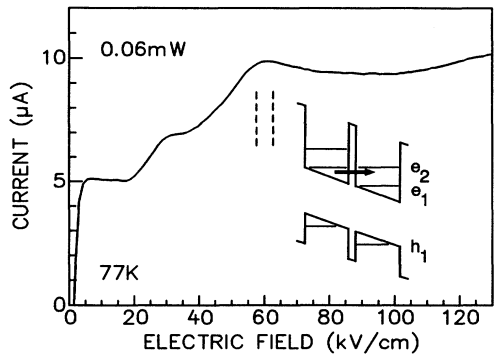

FIG. 3. Photocurrent versus electric field at 0.06 mW excitation power. The inset shows the situation when the $e1$ and $e2$ subbands are in resonance.

agrees with the field value where the ratio I_2/I_1 between the $e2$-$h1$ PL intensity I_2 and the $e1$-$h1$ PL intensity I_1 is maximized (see Fig. 2). In addition, a maximum in the photocurrent occurring in between the maximum of I_2 and the minimum of I_1 is also expected from particle conservation.

We briefly discuss the additional structures contained in Fig. 3, which are analogous to those of Fig. 2(b). The steplike structure in Fig. 3 at 5 kV/cm is related to miniband conduction. It appears at smaller fields than the corresponding structure in Fig. 2(b) because of the different space-charge influence. The step at around 32 kV/cm corresponds to phonon-assisted tunneling as mentioned above. The increase of the photocurrent above 100 kV/cm is partly due to enhanced nonresonant tunneling rates and to the $e1$-$e3$ resonance. It is not associated with avalanche multiplication processes which are only observed above 220 kV/cm.[10]

Time-resolved measurements of the photocurrent under pulsed optical excitation have been performed previously[4] in order to determine directly the resonance field for photocarrier transport. Although essentially the same resonance fields are obtained, the results are not directly transferrable to the present situation since the precise influence of the space charges in both experiments is presumably not identical.

IV. DISCUSSION

A. Influence of space charges on the resonance phenomena

A rate equation analysis of the transport and recombination processes in weakly coupled quantum wells results in the following relation[13] between the observed PL intensities I_1 and I_2 of the $e1$-$h1$ and $e2$-$h1$ transitions, respectively,

$$\frac{I_2}{I_1} = \frac{f_2}{f_1}\frac{\tau_{is}}{\tau_t} \ . \tag{2}$$

Here τ_1 is essentially the time constant for electron transport from one well to the adjacent well, τ_{is} is the intersubband relaxation time. f_1 and f_2 are the oscillator strengths of the $e1$-$h1$ and $e2$-$h1$ transitions. The ratio f_1/f_2 for different external voltages has been determined by photocurrent spectroscopy.[14] At the electric fields of interest here, the result can be expressed as[14] $f_1/f_2 = \alpha \exp(-F/\beta)$, with the coefficients $\alpha = 9.64$ and $\beta = 49$ kV/cm. Equation (2) was used previously to determine τ_{is}.[13] There the PL intensity ratio I_2/I_1 was measured under *pulsed excitation,* with an observed value of $I_2/I_1 = 0.4\%$ under resonance conditions, corresponding to an occupation ratio between the $e2$ and $e1$ subbands of $n_2/n_1 = (I_2/I_1)f_1/f_2 = 1.1\%$. In combination with $\tau_t = 60$ ps, as obtained from time-resolved photocurrent measurements,[10] an intersubband relaxation time of about 0.65 ps was found.

The pulsed excitation conditions of Ref. 13 differ from the present case where we use *stationary* optical excitation. In the experiment, this difference becomes evident from the field-dependent PL intensities of Figs. 2(a) and 2(b). In fact, both the $e1$-$h1$ and the $e2$-$h1$ PL intensities

I_1 and I_2 show a pronounced resonance behavior at around 60 kV/cm, giving maxima in the intensity ratio I_2/I_1 of 5.5% and 4% at 0.06 mW and 0.3 mW, respectively. Under nonresonant conditions, say, at about 80 kV/cm, we have $I_2/I_1 = 0.1-0.2\,\%$. In addition, the observed resonance minimum of I_1 is very sharp, with a full width at half maximum (FWHM) of 8 kV/cm (at 0.06 mW) and 7 kV/cm (at 0.3 mW). In contrast, a steplike field dependence of I_2/I_1 was found in Ref. 13, without any resonance minimum. The time-of-flight experiments in Ref. 10 give rise to a resonance FWHM of 22 kV/cm for the transport rates.

In order to explain these differences we consider the fact that the resonance field of a tunneling resonance is usually stabilized by space-charge effects. An experimental manifestation of this stability of resonant-field configurations has been given previously[15] by the observation of electric-field domains arising from a space-charge determined field distribution, where each field domain corresponds to a resonance field. In the present context, there is a space-charge density of about $(1-2)\times 10^{15}$ cm^{-3} in the undoped region already *without illumination* due to residual impurities, giving rise to a field inhomogeneity of 10–20 kV/cm across the intrinsic layer of the *p-i-n* diode. Such an inhomogeneity has also been discussed previously[10] since it will cause a broadening of the resonance behavior at small excitation levels. In addition, monolayer fluctuations of the well width may cause an additional inhomogeneity of the field values for resonant tunneling between adjacent wells.[8] The field inhomogeneity is now reduced under static illumination if the diode is biased close to resonance, thus giving rise to a sharpening of the field dependence of the resonance. This explanation is further supported by the enhancement of the resonance behavior of the $e1$-$h1$ PL intensity with increasing power as observed in Fig. 2.

In order to get further information on the field distribution across the MQW, we have analyzed in Figs. 4(a) and 4(b) the spectral position of the peak and the half-intensity energies of the field-dependent $e1$-$h1$ PL line. The overall redshift with increasing field is due to the quantum-confined Stark effect. The choice of the screening parameter α, as defined above, is justified from the agreement of the exciton peak energies between Figs. 4(a) and 4(b). The resulting values of α give evidence that space-charge effects actually play an important role.

Of particular interest is the regime close to resonance (around 60 kV/cm) where both the position and the width vary in a steplike manner. We note that this feature *cannot* be explained by a level repulsion, as observed in strongly coupled MQW,[3–5] since the signature of the latter is an additional redshift on the low-field side and an additional blueshift on the high-field side of the resonance, which is opposite to the present results.

Similar structure as in Fig. 4(a) has been observed previously by Tarucha and Ploog.[8] They attributed the anomaly to a spectral inhomogeneity of the PL quenching due to the tunneling resonance. Following their arguments, spatial fluctuations of the well width give rise to a spectral distribution of the luminescence intensity with the low (high) energy side arising from the wider (narrower) wells, and to a distribution of resonance fields with the low (high) field part of resonance fields arising from the wider (narrower) wells. Thus, close to resonance, the low (high) energy side of the PL spectrum is quenched at lower (higher) fields, thus explaining the observed steplike structure in Fig. 4. As a second explanation, field inhomogeneities from space charges due to residual impurities again generate PL lines distributed over a certain spectral range through their Stark shift. Here the low (high) energy portion of the PL spectrum is associated with the high (low) field regions of the field distribution, so that the low (high) energy part of the PL is suppressed at low (high) fields around the resonance.

The field-dependent $e1$-$h1$ PL peak energies and linewidths in Fig. 4(a) are consistent with both explanations. In addition to the steplike structure, which is observed exactly at the intensity minimum of the $e1$-$h1$ transition (see Fig. 2), there is a line narrowing on both sides of the step, thus indicating a preferential quenching

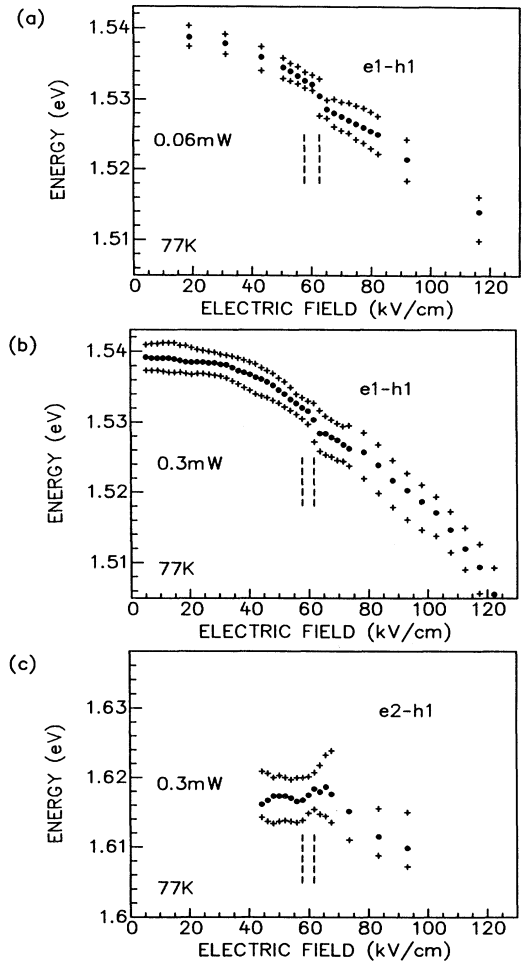

FIG. 4. Peak energies (●) and half-intensity energies (+) of the $e1$-$h1$ PL intensity at (a) 0.06 mW, (b) 0.3 mW, and (c) of the $e2$-$h1$ PL intensity at 0.3 mW, versus electric field. Dashed lines indicate the resonance fields obtained in Fig. 2.

of the low-energy and high-energy parts of the PL spectrum, respectively, slightly below and slightly above the step position. This line narrowing is more pronounced at the low-field side of the step, where the resonant maximum of the $e2$-$h1$ PL intensity is observed, than at the high-field side. As shown in Fig. 4(b), only the low-field line narrowing is still observed at higher excitation power. In addition, the field dependence of the step structure is now smeared out. The low-field resonances give additional structures in the energy positions and linewidths of Fig. 4(b) which will not be discussed further.

Under the conditions of Fig. 4(b), the $e2$-$h1$ PL was intense enough to perform a similar analysis, as shown in Fig. 4(c). At the field value of the $e2$-$h1$ intensity maximum (57 kV/cm), the $e2$-$h1$ position reaches a local minimum. There is a clear increase in energy by about 5 meV when approaching the field of the $e1$-$h1$ intensity minimum (62 kV/cm). Such increase is not unexpected from the previous discussion since, on increasing the field, selective quenching of $e1$ transitions with increasing energy should imply selective pumping of $e2$ transitions, again with increasing energy. Slightly above 62 kV/cm, there is a tendency of line broadening, which is not quite understood presently, probably arising from hot-electron effects. At higher fields, the Stark shift moves the $e2$-$h1$ transition towards lower energies.

B. Influence of the exciton binding energy

Although a variety of aspects has already been discussed, it is not yet clear what is the origin of the shift in electric field between the resonance minimum of the $e1$-$h1$ and the resonance maximum of the $e2$-$h1$ PL intensities. In *strongly coupled* quantum wells, resonance between subbands manifests itself in a level splitting[3–5] of the $e1$-$h1$ and the $e2$-$h1$ excitons due to the coherent interaction with the $e2$-$h1$ and $e1$-$h1$ transitions, respectively, of the right- and left-adjacent wells. However, the resonance splitting in the energy regime of the $e1$-$h1$ exciton is observed at larger fields than the resonance splitting of the $e2$-$h1$ exciton. This is the case because the resonance splitting is due to an avoided crossing of *exciton states,* not of pure conduction subbands. If E^x_{11d}, E^x_{11i}, E^x_{21d}, and E^x_{21i} denote the binding energies of the spatially direct and spatially indirect $e1$-$h1$ and $e2$-$h1$ excitons, respectively, the condition for the resonance splitting of the $e1$-$h1$ exciton is

$$|eFd| = E_{e2} - E_{e1} + E^x_{11d} - E^x_{21i} \ . \tag{3}$$

The resonance splitting of the $e2$-$h1$ exciton occurs at

$$|eFd| = E_{e2} - E_{e1} + E^x_{11i} - E^x_{21d} \ . \tag{4}$$

The corresponding energy configurations, though for the situation of weak interwell coupling, are indicated in Figs. 5(a) and 5(b), respectively. Since the binding energies E^x_{11d} and E^x_{21d} of the intrawell excitons are larger than those of the interwell excitons E^x_{11i} and E^x_{21i}, the resonance field of the $e1$-$h1$ transition is larger than the resonance field of the $e2$-$h1$ exciton by the amount

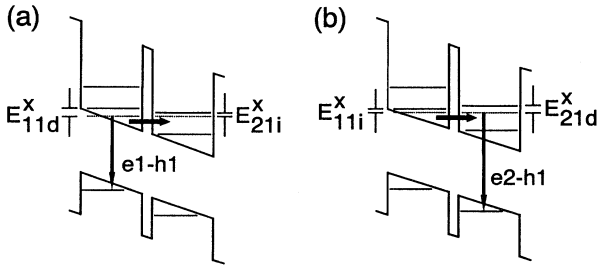

FIG. 5. Band diagrams of (a) the resonant damping of the $e1$-$h1$ luminescence and (b) the resonant pumping of the $e2$-$h1$ luminescence in weakly coupled MQW. E^x_{11d}, E^x_{11i}, E^x_{21d}, and E^x_{21i} are the binding energies of the spatially direct and spatially indirect $e1$-$h1$ and $e2$-$h1$ excitons, respectively (not to scale). Dashed lines indicate the energies of the excitons involving the $h1$ subband located in (a) the left quantum well and (b) the right quantum well, as counted from the respective valence subband energy.

$$\Delta F = \frac{1}{ed}(E^x_{11d} - E^x_{21i} + E^x_{21d} - E^x_{11i}) \ . \tag{5}$$

In Ref. 5, these binding energies were calculated for similar sample parameters (9.5-nm GaAs wells, 1.5–3.5-nm $Al_{0.3}Ga_{0.7}As$ barriers). The result $E^x_{11d} - E^x_{21i} \approx E^x_{21d} - E^x_{11i} = 4.0$–$4.5$ meV compares well with their experimental value of 5 meV. We note that the calculated binding energies of the interwell excitons are still relatively large (3.6–3.7 meV) although their oscillator strength is negligibly small.

The resonant alignment of exciton transitions, as already expressed in Eqs. (3) and (4), respectively, is shown schematically in Figs. 5(a) and 5(b). In contrast to the situation considered in Refs. 3–5 we do not observe a resonant splitting of excitonic absorption peaks in our present experiment. Instead, we are studying the influence of transport effects (shaded arrows in Fig. 5) on the intensity of the excitonic recombination (full arrows). If the experimental minimum of the field-dependent $e1$-$h1$ PL and the maximum of the $e2$-$h1$ PL (see Fig. 2) can be associated with the situations of Figs. 5(a) and Fig. 5(b), respectively, then the observed difference $\Delta F = 6$ kV/cm, i.e., $e\Delta Fd = 8.6$ meV, gives rise to a difference of about 4.3 meV between the binding energies of the intrawell and interwell excitons. [See Eq. (5)]. This value is in reasonable agreement with the theoretical values.[5] Consequently, such an assumption will quantitatively explain the experimental shift between the $e1$-$h1$ and $e2$-$h1$ PL resonance positions.

Therefore, it is important to discuss which of the situations outlined in Fig. 5(a), Fig. 5(b), and in the inset of Fig. 3 is relevant for a specific resonance phenomenon. In a photoconduction measurement, the resonance condition usually corresponds to the alignment of the conduction subbands, as depicted in the inset of Fig. 3. This is due to the fact that the drifting carriers are predominantly located in nonexcitonic states.

While the *motion* of all the carriers is seen in the pho-

tocurrent, *the excitonic PL only monitors carriers located in exciton states.* In order to identify the resonance behavior of the PL intensity, we therefore have to consider the field where the respective excitons are resonantly damped or pumped. For the intrawell $e1$-$h1$ exciton, the damping is expected to be strongest when the exciton energy is degenerate with the energy of the spatially indirect $e2$-$h1$ *exciton.* This argument suggests that Fig. 5(a) actually applies to the resonance minimum if the $e1$-$h1$ PL is monitored. Similarly, the intrawell $e2$-$h1$ PL is most strongly pumped if the energies of the intrawell $e2$-$h1$ exciton and of the interwell $e1$-$h1$ excitons are in resonance, as shown in Fig. 5(b). This mechanism relies on the efficient formation of spatially indirect $e1$-$h1$ excitons. Indeed, the rather large binding energy[5] of these interwell excitons reveals that the Coulomb attraction between carriers located in adjacent wells is still very strong. To summarize these arguments, the apparent field position of the $e1$-$e2$ tunneling resonance, as observed in the field dependence of the photocurrent, the $e1$-$h1$ PL, and the $e2$-$h1$ PL, is given by Eqs. (1), (3), and (4), respectively, and corresponds to the situation outlined in the inset of Fig. 3, in Fig. 5(a), and Fig. 5(b). Consequently, the measured resonance field does not only depend on the subband spacing and on the MQW period, *but also on the measurement method.*

V. CONCLUSION

We have studied the influence of resonantly enhanced tunneling rates in weakly coupled MQW's on the intensities of the excitonic photoluminescence, involving the initial conduction subband $e1$ and the final conduction subband $e2$, and on the photocurrent. Each of these experimental probes gives rise to a slightly different field position where the resonance arising from the energetic alignment of the $e1$ and $e2$ states is observed. We discuss these differences in the resonance field value as an evidence for excitonic effects giving rise to a shift of the resonance minimum of the $e1$-$h1$ PL towards higher fields and to a shift of the resonance maximum of the $e2$-$h1$ PL towards lower fields, both with respect to the resonance field as determined from the photocurrent. The observed magnitude of this shift is consistent with calculated differences[5] in the binding energies of direct (intrawell) and indirect (interwell) excitons. In addition, these results give evidence for the contribution of interwell excitons to the transport phenomena. Our experiments therefore provide a method to study these interwell excitons which cannot be studied directly by optical methods, namely, by their influence on the luminescence of intrawell excitons.

ACKNOWLEDGMENTS

The authors are grateful to H. T. Grahn (Berlin) for helpful discussions. Thanks are due to P. Koidl (Freiburg) for encouragement of this work. We also acknowledge partial support by the Bundesministerium für Forschung und Technologie.

[1]E. E. Mendez, F. Agulló-Rueda, and J. M. Hong, Phys. Rev. Lett. **60**, 2426 (1988).
[2]P. Voisin, J. Bleuse, C. Bouche, S. Gaillard, C. Alibert, and A. Regreny, Phys. Rev. Lett. **61**, 1639 (1988).
[3]A. M. Fox, D. A. B. Miller, G. Livescu, J. E. Cunningham, J. E. Henry, and W. Y. Jan, Phys. Rev. B **42**, 1841 (1990).
[4]H. Schneider, H. T. Grahn, K. v. Klitzing, and K. Ploog, Phys. Rev. Lett. **65**, 2720 (1990).
[5]A. M. Fox, D. A. B. Miller, G. Livescu, J. E. Cunningham, and W. Y. Jan, Phys. Rev. B **44**, 6231 (1991).
[6]F. Capasso, K. Mohammed, and A. Y. Cho, Appl. Phys. Lett. **48**, 478 (1986).
[7]S. Tarucha, K. Ploog, and K. v. Klitzing, Phys. Rev. B **36**, 4558 (1987).
[8]S. Tarucha and K. Ploog, Phys. Rev. B **38**, 4198 (1988).
[9]H. Schneider, K. v. Klitzing, and K. Ploog, Superlattices Microstruct. **5**, 383 (1989).
[10]H. Schneider, K. v. Klitzing, and K. Ploog, Europhys. Lett. **8**, 575 (1989).
[11]H. Schneider, W. W. Rühle, K. v. Klitzing, and K. Ploog, Appl. Phys. Lett. **54**, 2656 (1989).
[12]G. Livescu, A. M. Fox, D. A. B. Miller, T. Sizer, W. H. Knox, A. C. Gossard, and J. H. English, Phys. Rev. Lett. **63**, 438 (1989).
[13]H. T. Grahn, H. Schneider, W. W. Rühle, K. v. Klitzing, and K. Ploog, Phys. Rev. Lett. **64**, 2426 (1990).
[14]H. T. Grahn, W. W. Rühle, and K. Ploog, in *Quantum Well and Superlattice Physics IV,* edited by G. H. Döhler and E. S. Koteles, SPIE Conference Proceedings No. 1675 (International Society for Optical Engineering, Bellingham, WA, 1992), p. 36.
[15]H. T. Grahn, H. Schneider, and K. v. Klitzing, Appl. Phys. Lett. **54**, 1757 (1989).